Measurements of a Three-lens Light Collector

Reinhard Eckmann, Michael Ispirian, Suren Karabekyan,
John McGill, Roy Schwitters

September 1997

1 Introduction

A sample light-collecting telescope was assembled from three, identical WAHL
company lenses and its properties were studied in an experimental setup.
The aim of the study was to gain experience with quality-control and testing
techniques that will be used with the future two-lens telescopic light collector
for the RICH photon detector. We are able to simulate the observed per-
formance of this system with design tools developed for the Hera-B RICH
light collectors.

2 Experimental Setup

2.1 The telescope

The telescope was assembled from one field lens and a pair of condenser
lenses, which were positioned in holders. All three lenses are of the same
type. The holders can slide along three metallic rods running parallel to
the optical axis, and their position can be aligned and fixed along the rods.
Masks or diaphragms can be put on top of the telescope. In addition, a flat
mirror, used for alignment, can be put on top of the field lens.

The distances between the lenses of the telescope and the photocathode
of the PMT were set to the calculated values. In this calculation, radii of
curvature of the lens surfaces $R_1 = 77$ mm and $R_2 = 47$ mm and refractive
index equal to 1.505 were assumed. During the studies, it was thought that
these radii were 81.1 mm and 44.5 mm, respectively. In spite of the differ-
ence, the lens positions were kept the same to make the studied properties
comparable with calculations. As discussed below, the lenses were subse-
quently measured to determine their actual shape; parameters derived from

1

these measurements were used in simulation studies and are presented in that section. In summary, the properties of the telescope assumed in the setup and measurements presented here are:

- Focal length of one lens: ≈ 45 mm

- Diameter of one lens: 37 mm. Diameter of a lens holder's opening: 35.9 mm.

- Refractive index of the lens material taken equal to 1.505 in calculations

- Axial positions of the lenses in mm:

Surface	Position, mm
Field lens, first surface	0
Field lens, second surface	7
Condenser lens 1, first surface	91
Condenser lens 1, second surface	98
Condenser lens 2, first surface	99
Condenser lens 2, second surface	106
PMT entrance window	144.2

- Magnification (nominal): –0.5

- Total length (from the field lens to the image plane): ≈ 145 mm

An M16 photomultiplier tube was placed at the expected image plane. When placing the PMT in its longitudinal position, the influence of the thickness of the input glass window — an additional 0.8 mm shift towards the telescope — was taken into account.

The telescope can be removed out of the setup, leaving only the PMT under illumination. This is necessary for collection-efficiency measurements as well as studies of angular dependencies.

2.2 The test setup

The telescope with the PMT was placed in a dark box with its axis vertical. Two light sources, a deuterium lamp for UV range and a tungsten lamp for visible range, were used as light sources to a monochromator. See Figure 1. A detailed description of the light sources and the monochromator is given in the paper *Measurements of Transmission of Plastic*. A beam "parallelizer" was added to this setup to provide a homogeneous and parallel light beam with a diameter of 90 mm for illuminating the field lens.

1 mm
Diaphragm
F=660mm
Metallic mirror
Metallic mirror

Mono-
chromator

Quartz lens
Diffuser

90

Dark box

Alignment mirror;
removed after alignment

Telescope

M16
PMT

Top view of the mirror part

Rotation axes

Telescope

Cables

Light seal

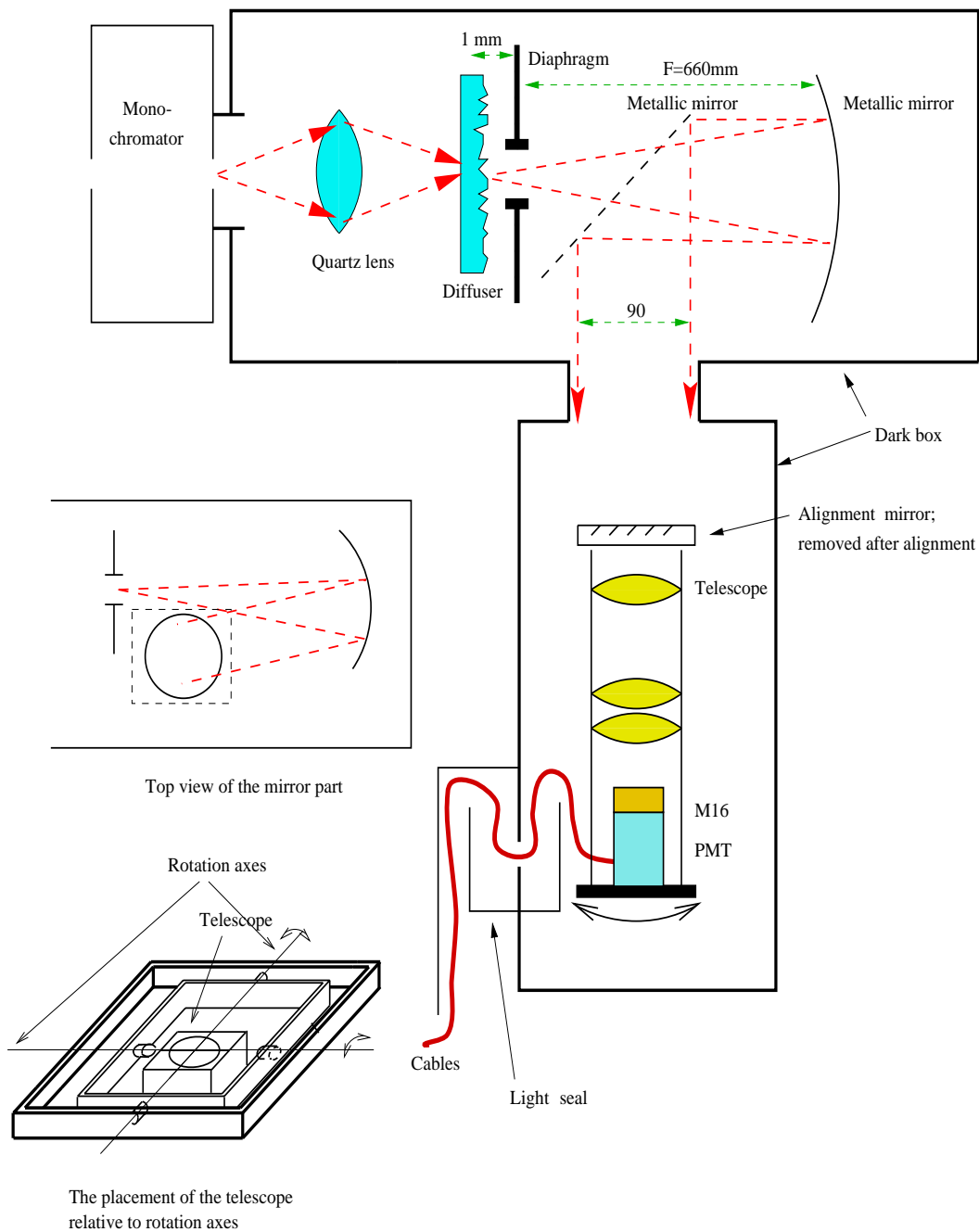The placement of the telescope
relative to rotation axes

Figure 1: The test setup. Picture is not to scale.

The optics of the test setup works as follows:

The output light from the monochromator is collected with a quartz lens and focused on a diffuser. A small diaphragm right after the diffuser masks the major part of the illuminated area of the diffuser, allowing only 1 mm circle to emit light further. The diaphragm is in the focal plane of a parabolic Al mirror, which transforms the light into an almost parallel beam. This beam is then reflected downwards by a flat mirror, illuminating the telescope.

The role of the diffuser is threefold. First, it broadens the angular spectrum so that the entire aperture of the subsequent optics is filled. Second, the diffuser's output has a homogeneous distribution over the lateral coordinate and an angular spectrum, independent of the monochromator's output, which makes it possible to obtain a homogeneous parallel beam for the telescope study. These positive effects are offset by the third, undesireable property, an unavoidable decrease of intensity. Great care was taken in the preparation of this optical system to find an appropriate compromise.

The diameter of the output beam is larger than the field lens; thus, the latter is fully covered. The divergence (angular uncertainty) of the resulting "parallelized" beam is $\approx \pm 2$ mrad. This value is mainly determined by the size of the opening of the diaphragm (cannot be made smaller since the intensity drops) and by aberrations of the parabolic mirror.

In the dark box, the telescope is mounted on a movable platform, allowing rotations along two axes. Declination angles up to ± 160 mrad are achievable. The uncertainty of the angular position is known with accuracy better than 0.5 mrad.

To minimize the movement of the telescope position during the rotation, the center of the field lens is at the point where the two rotation axes cross. Thus the spatial position of the field lens center is maintained during the rotation, preventing it from going out of the illuminating beam.

A Hamamatsu R5600-M16 photomultiplier tube is used for the photon detection. It is plugged into one of 2×1 RICH baseboard prototypes. Two ASD8 boards, necessary to read the signals from one PMT, were used in the setup. The cables from the ASD8 boards run through a labyrinth-like appendix on the wall of the dark box to prevent room light entering the box.

The output of the ASD8 boards is read-out by two VME modules, which convert the signals to NIM standard. After, the signals are read by a VME scaler.

For further reference, the scheme for identifying channels of the PMT and the directions of axes are shown in Figure 2.
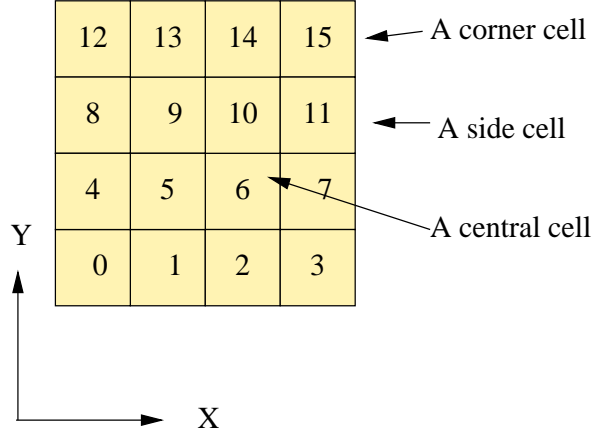
Figure 2: Numbering of channels and direction of axes

2.3 Alignment of the setup

The whole setup was aligned relative to the incident light beam prior to the measurements.

The telescope's mechanics was designed in a way which allows individual alignment of the lenses. The position of the field lens was fixed relative to three rods providing the telescope's mechanical structure. The positions of the other two lenses and the PMT were set by a caliber and fixed by nuts on the threaded rods.

The first alignment of the setup is the centering: assuring, that PMT's center is on telescope's axis. This alignment was done outside of the box, by shining a laser beam through a small centered diaphragm placed on top of the field lens and by observation of the spot on the PMT's surface. The body of the tube was shifted until the spot came to the center of the PMT. The size of the spot on the PMT is 0.25 mm.

In the next step, the field lens of the telescope was fixed perpendicular to the incident light. This alignment was done by putting a flat mirror on top of the field lens parallel to the lens and by observation of the light, which is thus reflected back. The light goes the same path as the incident light, but in the opposite direction, and focuses to a spot in the diaphragm's plane (the diaphragm stands right after the diffuser, see Figure 1). If the mirror is really perpendicular to the incident light, then the spot is inside the opening of the diaphragm and for this reason is invisible. Otherwise, a spot is seen on the right-hand surface of the diaphragm, and the telescope is rotated

5

until the spot goes inside the opening. The parallelism of the middle surface of the field lens and the alignment mirror was achieved through a proper mechanical design of the telescope. This step of alignment procedure was done with laser light, because the monochromator's output is too weak to see.

After that the telescope was removed, and the same procedure with the back reflection of the light was done with the PMT: its entrance window was aligned perpendicular to the incident light through shifts in its mechanical holding.

Finally, since the alignments are not quite independent, the steps of alignment were repeated. One–two iterations appeared to be enough. The achieved angular accuracy of the alignment is estimated to be 3 mrad. The lateral misalignment is estimated to be 0.4 mm. This quantity includes the shift of the spot due to lateral shift of lenses in the telescope (shift of the spot is of the same magnitude as the lens shift).

2.4   Stability of the light sources and of the PMT readout

The basic measurements described further in this paper take from one to twenty minutes to accomplish one step. That for, the long-term stability of the light sources, the PMT and the readout system was studied before the measurements. An alternative could be the usage of a monitor PMT, but the PMT's characteristics themselves as well as the sensitivity of the readout system could drift. Although, a monitor PMT could almost totally remove the influence of the drift of the light sources. However, the setup does not include a monitor PMT, since the one that was initially planned to be used appeared to be defective, and the delivery and preparation time of another would be too long.

Because of drifts, it is desirable to accomplish one measurement as quick as possible. Since the procedure, as a rule, includes opening of the dark box and subjecting of the PMT to daylight, the "rest" characteristics of the PMT was studied: the reduction of the background rate after bright illumination (no high voltage during illumination, naturally). The aim of this study was to find the necessary amount of time one shall wait before data taking after the light sources are switched on or the dark box is opened.

It appeared that the background resting time is close to 15 minutes, as it can be seen in Figure 3.

If the initial illumination was not bright but rather ordinary room illumination or even attenuated, then the rest time was several times smaller. In all cases, after 10 minutes the mean background rate was less than 40
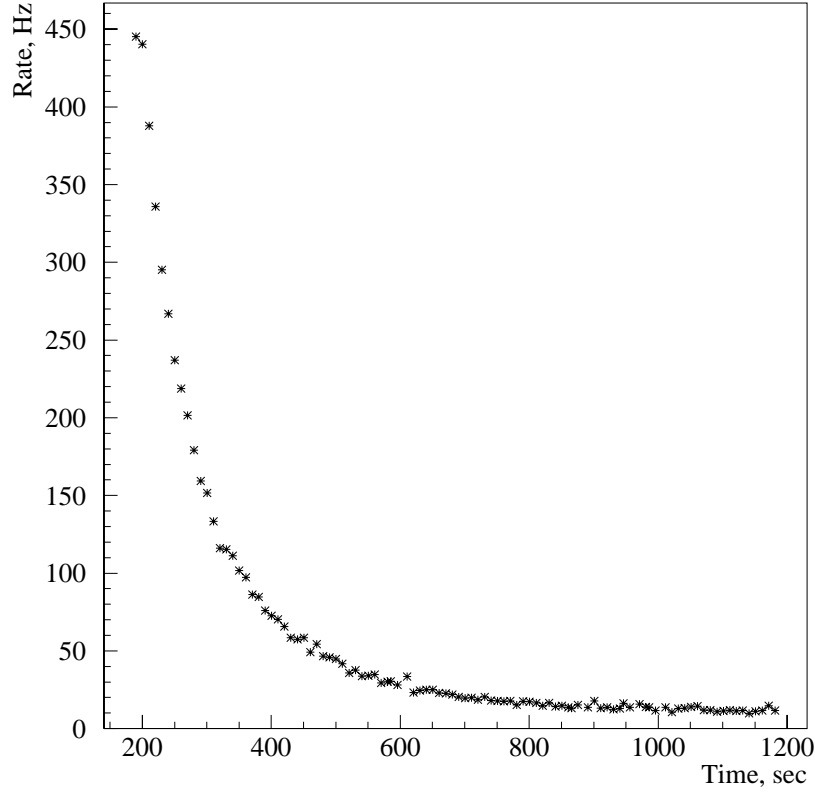
Figure 3: Decrease of the background rate in darkness. Mean rate in channels.

Hz. Our data on rest-time coincides with that brought in the Ljubljana note *Quality assessment tests of Hamamatsu M16 photomultipliers.*

There are two main light sources in the setup: a deuterium lamp, covering spectral range $260 - 400$ nm, and a tungsten lamp, covering the range $400 - 600$ nm. The following Figure 4 shows their stabilities beginning from the moment of switching on. Data taking period is 1 minute. Naturally, the curves represent not only the stability of the photon flux, but also the drift of the PMT's properties and of the further signal processing chain.

Conclusion: the drift over the measurement duration of 20 minutes is smaller than 0.8% after a proper waiting time of 30 minutes.
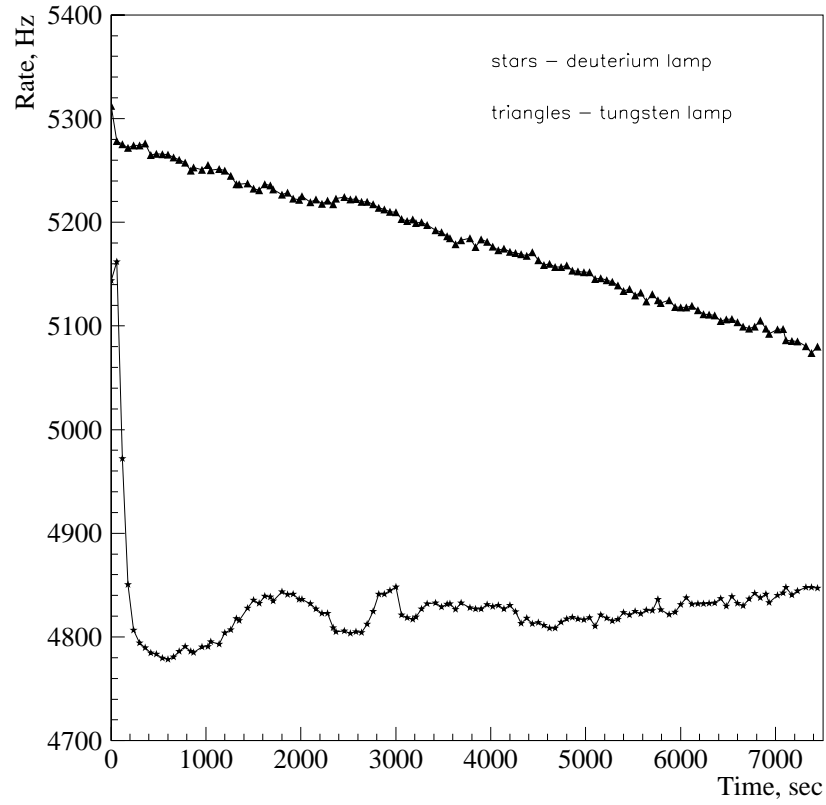
Figure 4: Stability of the two light sources

To monitor the drift, before and after a measurement, two reference rates were measured under fixed conditions: one with deuterium lamp and the other with tungsten lamp. An example of a reference measurement is shown in Figure 5. Due to small deviation from constant value, no correction of the measured rates of channels is necessary.
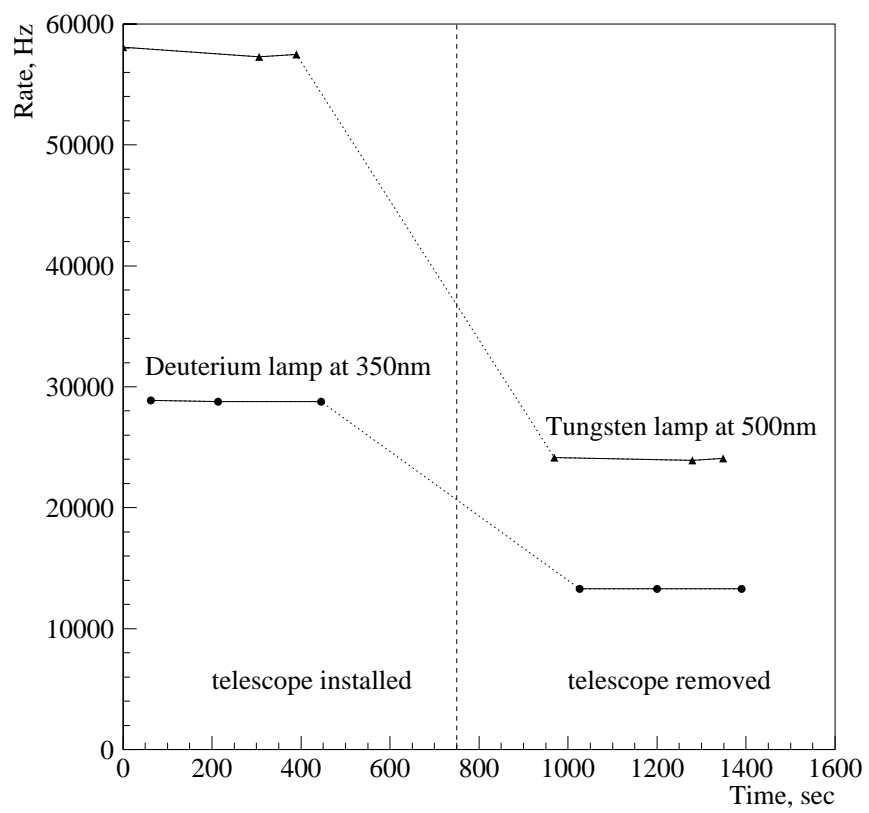
8

Figure 5: A reference measurement

3 Measurements

3.1 Test of imaging quality

To estimate the imaging quality of the telescope, two tests were carried out. The first simple test was accomplished outside the dark box: the shift of a spot image was studied versus incidence angle at fixed incident place.

A plate with three small holes, functioning as a light diaphragms, was positioned on top of the field lens, and centered. The holes were made in the center, at 7.5 mm apart from the center and at 15 mm apart. All holes lie in one line parallel to X axis. The incident narrow beam (red He-Ne laser at 633 nm, refractive index at this wavelength 1.488) was in XOZ plane. All three holes were illuminated in three sets of measurements, during each of those the angle was scanned. See Figure 6.
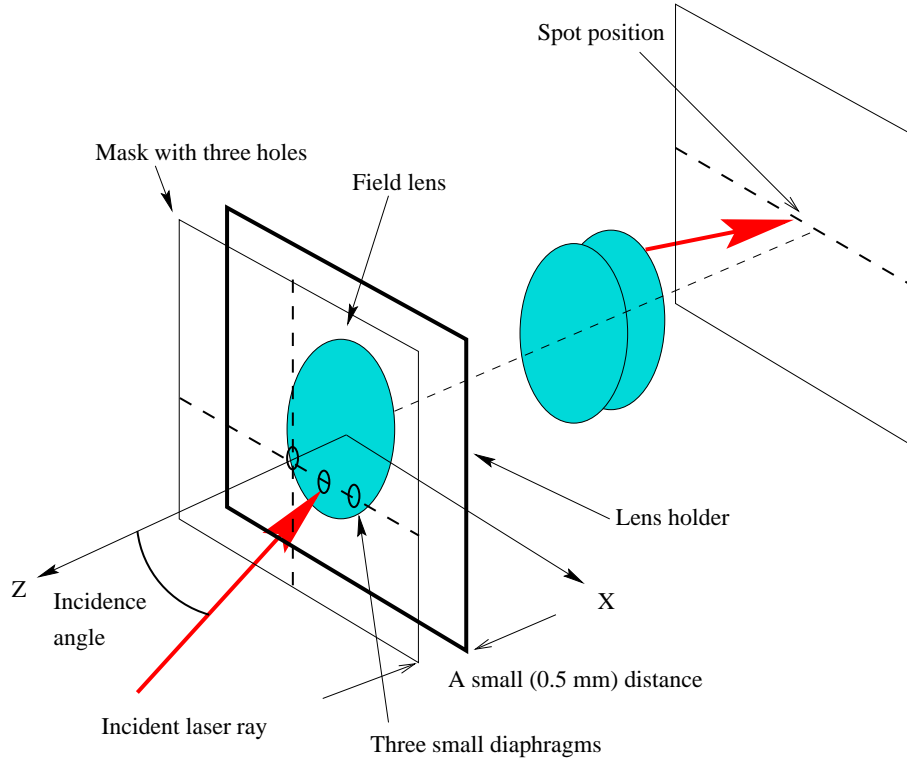

Figure 6: The scheme of spot scan experiment

The plots, showing the position of the spot at the PMT's window, are given in Figure 7, Figure 8, Figure 9. Note that for an ideal telescope there

10

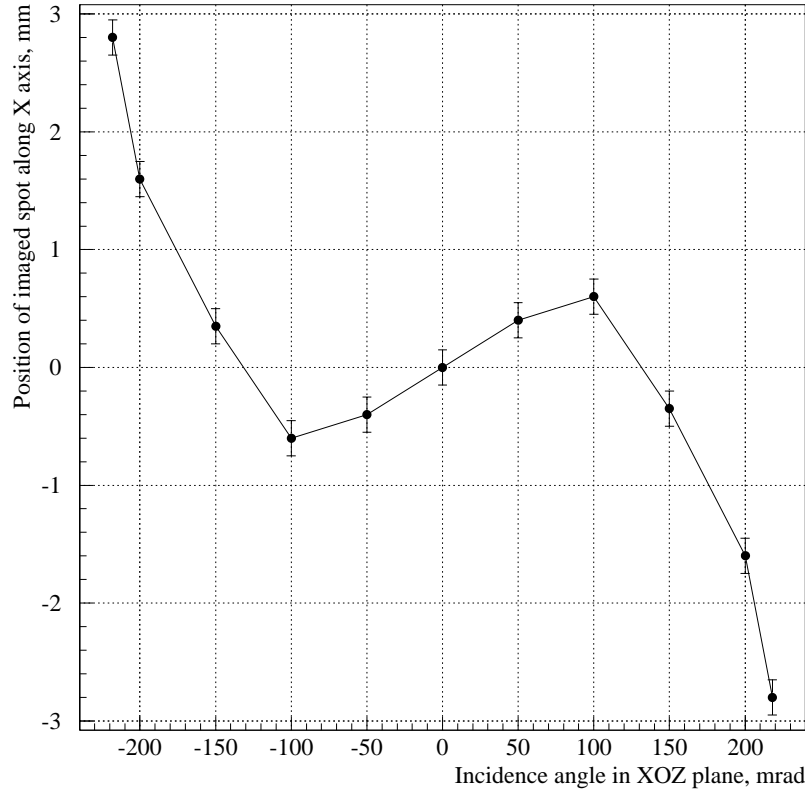should be no movement of the spot versus angle.

Figure 7: Shift of spot versus incidence angle for central incidence position

As one can see, the shift in the center is smaller than 0.5 mm for expected angular spectrum, which is quite acceptable. At half of the radius it is less than $\approx$ 1 mm. At the edge it reaches much higher values and goes out of acceptance.

The second test was also done outside the dark box: the image of of a regular array of crossed lines or grating was fixed on a photographic film.

The array had a pitch of 2 mm and was placed on top of the field lens. The film was placed at the location of the best visual focus. The light source used was red laser, the light of which was made parallel and falling with zero incidence angle. See Figure 10. The small red (or grey on black-and-white
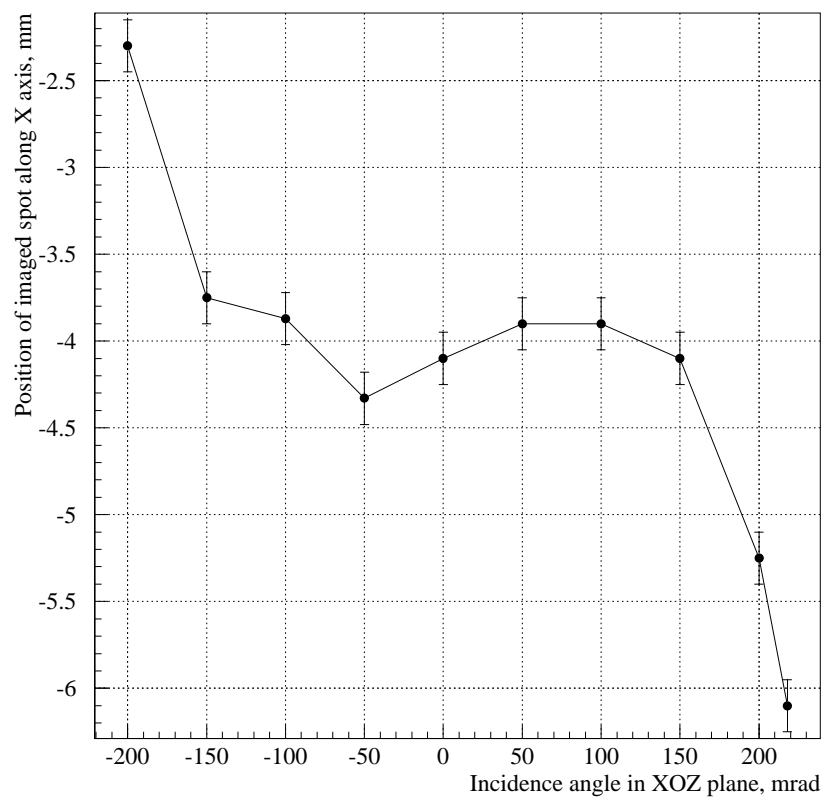
11

Figure 8: Shift of spot versus incidence angle for 7.5 mm incidence position
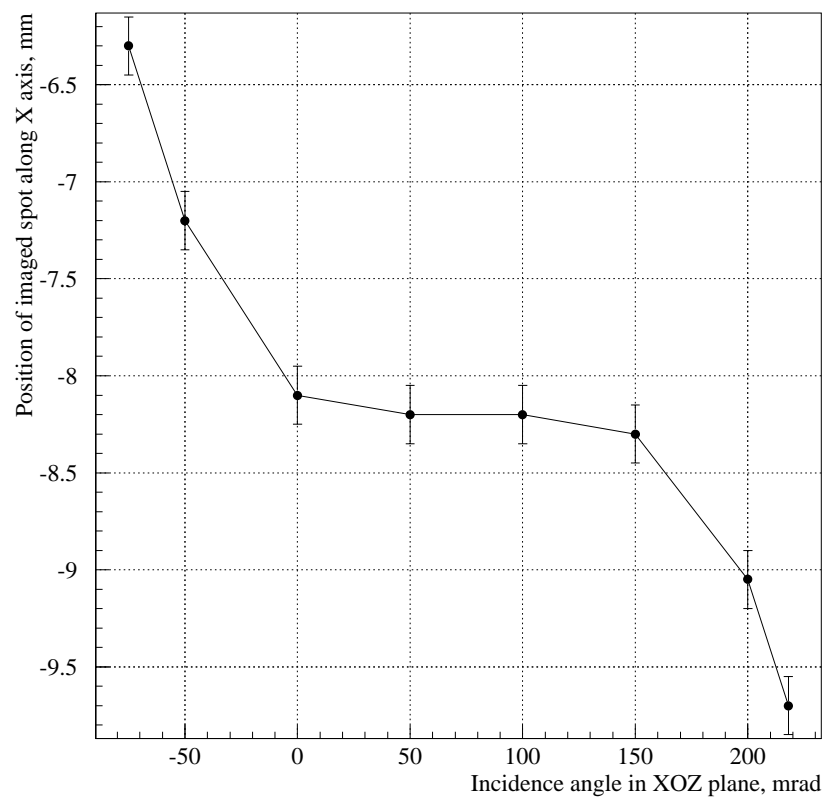
Figure 9: Shift of spot versus incidence angle for 15 mm incidence position

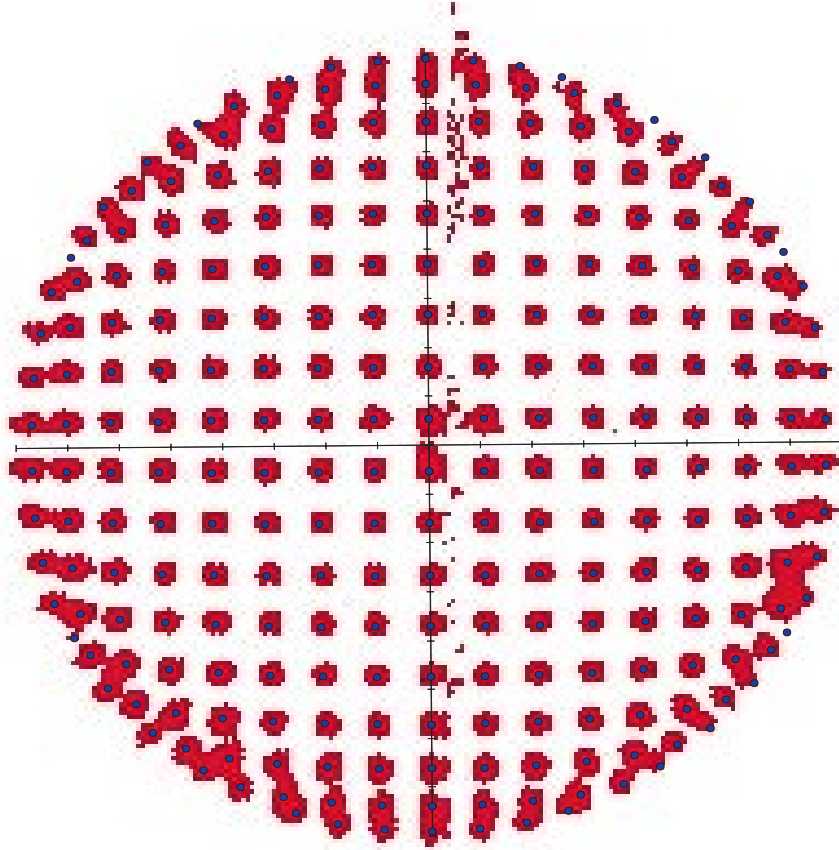copies) squares correspond to the open areas of the grating.

Figure 10: Photograph taken of 2 mm pitch grating (red) with simulated rays (blue dots), discussed below. Tic-marks indicate 1 mm scale on image plane.

For an ideal telescope, the image should also be a regular grid with square cells. The telescope clearly distorts the image, especially on the edges. A calculation was carried out to produce the array of dots superimposed on the image in the figure. As discussed below in the section on simulations, matching the actual image with the calculated array was crucial in determining deviations of actual lens parameters from expected values.

3.2 Collection efficiency of the telescope over the spectrum

The collection efficiency (transmission) of the channels as well as the mean collection efficiency of all channels was measured by taking the rates with installed telescope and without the telescope. The incidence angle is zero for this measurement. The definition of the collection efficiency we use:

$$\text{Collection efficiency} = \frac{(\text{rate with telescope}) - (\text{noise rate})}{4 * ((\text{rate without telescope}) - (\text{noise rate}))}$$

The factor 4 comes from the nominal magnification factor -0.5.

Collection efficiencies are shown in Figure 11.

A control measurement was done: in the range $380 - 400$ nm, where the emissions of two lamps overlap, the collection efficiency was measured with both lamps. The difference is less than 0.5% and is within the errors of the measurement.

The instability of the light sources is the dominating error in the collection efficiency measurement. At the wavelengths of measurement 300 and 310 nm the noise (or, to be more exact, the instability of noise) adds its statistical contribution to the measurement error, which is significant only for these two wavelengths. Other errors are much smaller and difficult to estimate. The error bars on the collection efficiency curve in Figure 11 represent the 0.8% lamp intensity drift and the said statistical error, multiplied by $\sqrt{2}$ because the value of collection efficiency is obtained through division of two measurements' data. We do not multiply the 0.8% by 2 but rather by $\sqrt{2}$, because under "error" we understand the standard deviation σ, calculated as sum of squares: $\sigma_{\text{coll. eff.}} = \sqrt{\sigma^2_{\text{without tel.}} + \sigma^2_{\text{with tel.}}}$.

A Monte-Carlo calculation of collection efficiency was performed prior to the detailed simulation studies discussed below. The results are shown in Figure 11as dashed lines. Substantial disagreement was observed, which provided the impetus for the later simulation studies.

3.3 Collection efficiency versus incidence angle

The telescope, together with the PMT, was inclined relative to incident light to study the dependence of the collection efficiency on the incidence angle. Two stepper motors and the rotation mechanics allow to make an angular scan in the range $\pm$ 160 mrad in each direction in one run.

The incidence angle over the PMT's surface is approximately twice large, than that over the field lens, and has the opposite sign. That for the angular sensitivity of the PMT was first studied. It appeared, that the sensitivity of
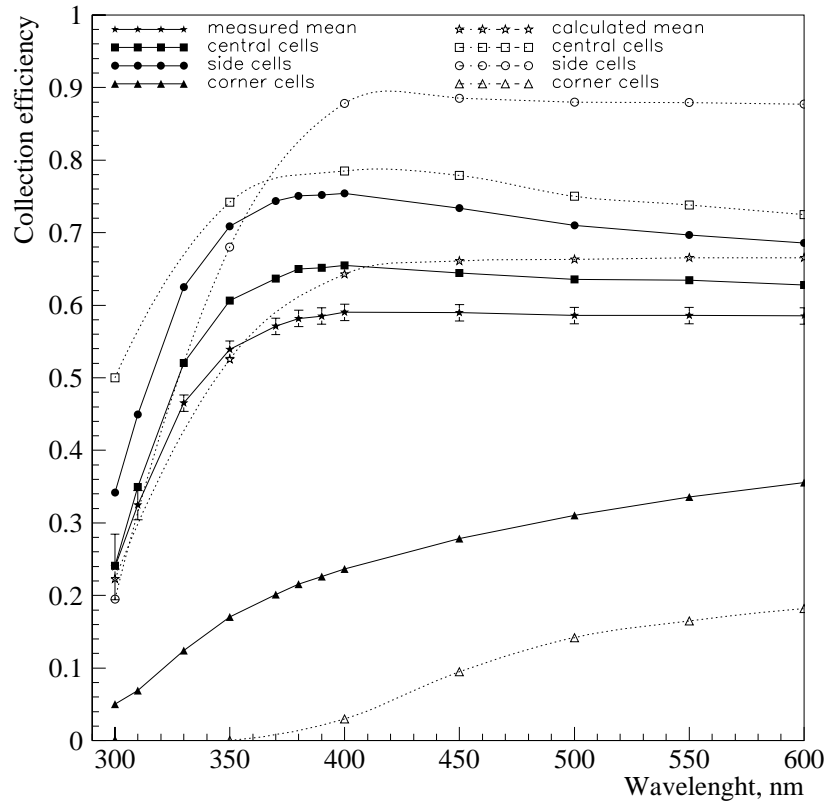
Figure 11: Collection efficiency of the telescope versus wavelength. Solid lines show the measurement data, dash lines show Monte-Carlo simulation data.

the PMT varies within several percents for the angular range of incident light −150 .. +300 mrad and has a maximum not always at zero degree incidence. Some examples of angular sensitivity of different tubes are shown in the following Figure 12, Figure 13, Figure 14. Because of unknown polarization of the incident light and other reasons as well it is difficult to interpret this data.
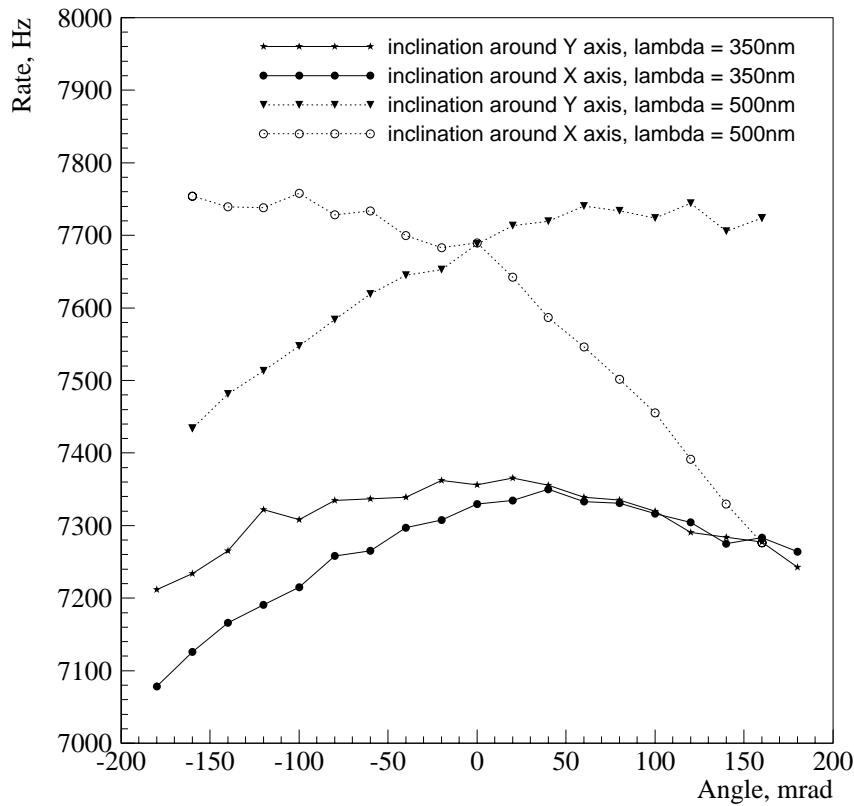

Figure 12: Angular sensitivity of the tube serial number 6L05RA

When calculating the collection efficiency versus incidence angles, the zero incidence angle signals in 16 channels were taken as denominator in the formula for collection efficiency determination, since there is a rather wide angular spectrum falling over the PMT.

In Figure 15 the collection efficiency is shown for incidence angles varying
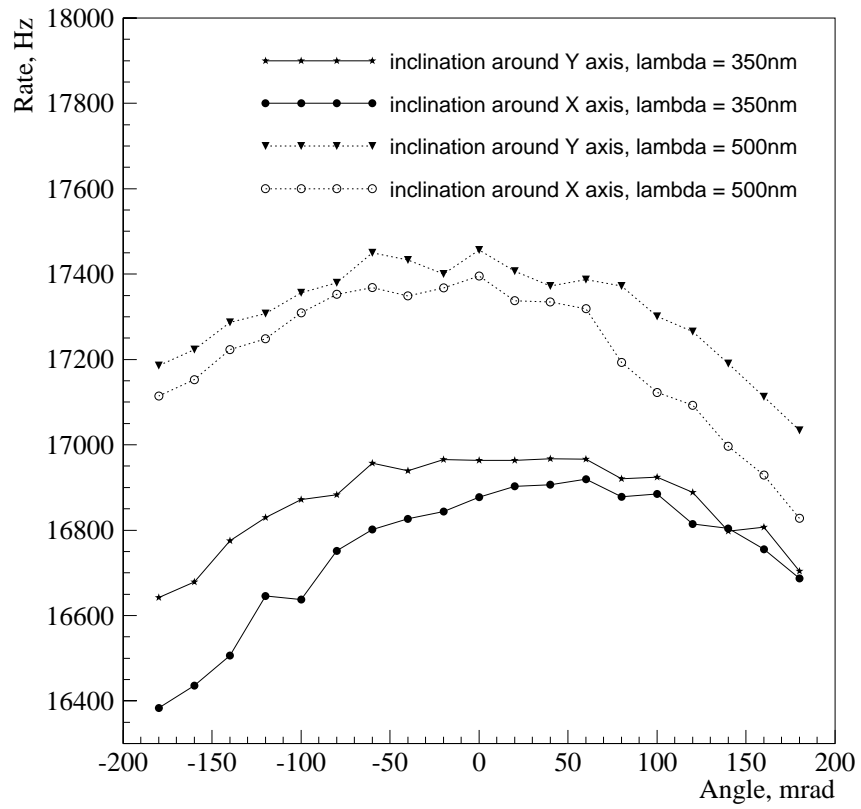
17

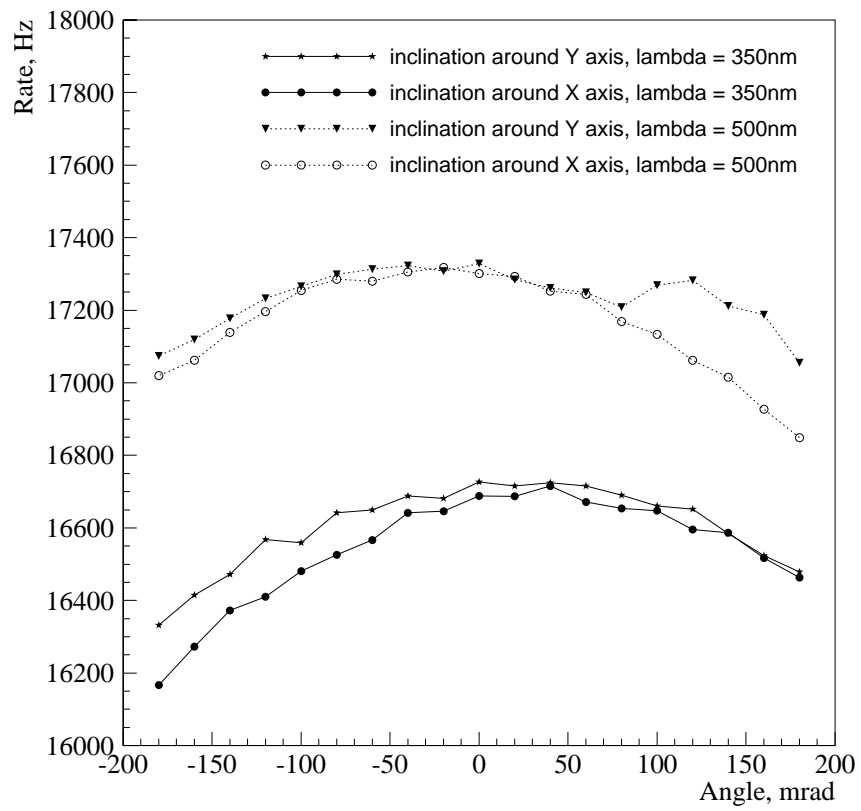Figure 13: Angular sensitivity of the tube serial number 6L26R7

Figure 14: Angular sensitivity of the tube serial number 6L29C4

in XOZ plane (the rotation axis is Y). Wavelength is 350 nm.

ANGULAR DEPENDENCE OF THE TELESCOPE TRANSMISSION
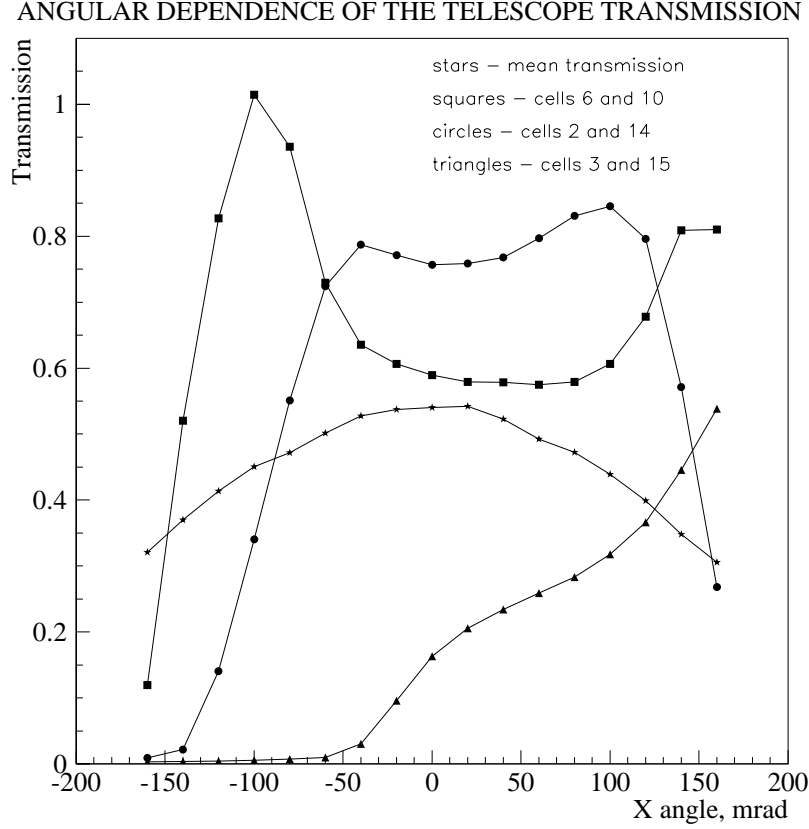
Figure 15: Collection efficiency of the telescope versus incidence angle

For an ideal telescope on focus, there should be no angular dependence of the collection efficiency. The decrease of the mean collection efficiency with the increase of angle is due to sliding of the whole picture out of the PMT. The increase of collection efficiency for some cells is due the shift of the spot, which increases with the angle: when inclined, the cells begin to receive the light, which went to neighbor cells at zero angle.

3.4 Study of multiple reflections and scattered light

There are seven uncoated reflecting surfaces in the setup: six of the lenses and one of the input window of the PMT. Besides, some diffuse scattering of light because of bulk and surface inhomogeneities is observed. That for, a study was performed to estimate the magnitude of reflections and scattered light.

The method chosen was to illuminate the telescope with a narrow beam and register the signals in the channels. In the absence of reflections and scattered light, only signals in the cells, which are directly illuminated with the narrow beam, should be larger than the dark rate. Total number of such cells, evidently, is $1 - 4$.

To obtain the narrow beam, a 3-mm diaphragm was placed on top of the field lens. It was positioned so, that at zero incidence angle the image was formed on the cross of the cells # 4, 8, 5 and 9.

The diaphragm was not positioned on the axis of the lens system, since the reflected photons right in the center go along the same path (because of normal incidence) with the main light and would be thus masked.

The image of the diaphragm on the PMT is ≈ 1.5 mm in diameter. This size could not be further reduced for two reasons: the inhomogeneous sensitivity of the photocathode even within one cell manifests itself too strong, and the absolute intensity becomes so small that the reflections are lost in the noise.

The illumination for this study was not the light from the monochromator (is too weak), but the filtered through a blue filter light of an incandescent tungsten lamp. The spectral range is estimated to be $350 - 450$ nm, which includes the wavelength range, where maximum of signal in RICH detector is expected. The light was as parallel as the light with monochromator.

An angular scan was performed in the range -160 .. $+160$ mrad. The results of this study must be treated as approximate only, for several reasons: (i) the amount of registered reflected and scattered light depends strongly on diaphragm position (this statement is also based on visual observation of the reflections with laser beam); (ii) it is not always possible to distinguish between the diffusely scattered and the reflected light; (iii) the study was done with broad-spectrum light, meanwhile the absorption, which is spectrally dependent, plays an important role in the study. A summary of results follows:

Study of the scattered light: the illumination through the diaphragm caused a noticeable, although small, increase of background in all channels.

In darkness, typical rates are $5 - 50$ Hz. With illumination, the rates in not directly illuminated channels increased up to $300 - 1500$ Hz, with the rates in illuminated channels being $\sim 10^4 - 10^5$ Hz. For two characteristic cases: zero incidence angle and 40 mrad angle in Y direction, the four illuminated cells contain $\approx 97\%$ of the total rate; the remaining 3% is in other 12 cells. These 3% include, naturally, not only the diffusely scattered, but also the multiple-reflected photons.

Study of the multiple reflection: for almost 2/3 of points of the scanned angular range, higher intensity in some 1–3 channels (besides the four directly illuminated channels) was detected. This is, evidently, due to reflections in the optical system. A typical example is shown in the following table, where rates are normalized to the rate in channel # 9 and the individual sensitivity of channels is accounted for.

Ch.	Rate	Ch.	Rate	Ch.	Rate	Ch.	Rate
0	0.006	1	0.005	2	0.003	3	0.022
4	0.699	5	0.678	6	0.005	7	0.003
8	0.655	9	1.000	10	0.006	11	0.004
12	0.010	13	0.015	14	0.022	15	0.004

One can see a noticeable increase in rates of channels # 3 and 14. Cell # 13 also has a little higher rate (compare with, say, cell # 6, which is at the same distance from the illuminated cells). When the multiple reflection is estimated numerically, it still lies within the 3%, which occupies the scattered light: as it was said before, the reflections and scattered light cannot be fully separated.

So, the conclusion: the scattered and multiple-reflected photons are observable. Total amount is of order of 3% (this value is obtained via looking through many of similar tables). Reflections are usually observed in 0–4 cells.

In the future two-lens setup, the number of reflecting surfaces will be reduced by two. But in the RICH detector this number will again increase by two because of the photon detector window.

4 Simulation of Optical Performance

This section describes our efforts to model the performance of the three-lens prototype light collector described above. The purpose is to check our understanding of such light collectors in preparation for production of the Hera-B RICH photon detectors. We use MS Excel optics tools developed for this purpose.

4.1 Procedure

The original design parameters that guided the experimental setup were found to not adequately describe the data—qualitatively, the image formed in the prototype setup was smaller than predicted (greater de-magnification) and appeared to be formed behind the expected focal plane. There are enough degrees of freedom in even this simple optical system that we can vary some from the design values and reproduce, reasonably well, the experimental observations. However, no set was obviously superior to all others. Therefore, after trying several approaches, we had to make judgments on the reliability of the relevant pieces of information and settled on the following steps to arrive at the model parameters presented here:

1. We fitted measurements of the lens surface dimensions to determine shape parameters (curvature and a 4th-order correction term) for both faces of the lenses. The three lenses are assumed to be identical.

2. We assumed the index of refraction for red laser light is 1.488. Several independent product curves from different manufacturers give this value. (The measurements of cell efficiencies were performed over a range of wavelengths; the corresponding values of index-of-refraction were taken from the manufacturers curves, which are well represented over the wavelengths of interest by the expression $n(\lambda) = 1.476 + (\frac{68.9\,\text{nm}}{\lambda})^2$.)

3. We varied: a) the separation between the first ("field") lens and second (first member of "condenser pair") and, independently, b) the separation between the third lens and the image plane in order to reproduce a photograph taken of a grating placed in front of the field lens.

4. We checked the optical parameters thus determined by comparing to the incident angle versus final position measurements given in Figures 7, 8, and 9 above. The position of the image plane was varied for

these studies, but a single z-location was used for all three initial beam positions.

5. We simulated the PMT cell efficiencies, quoted in the draft note, using optical parameters developed above, but varying the position of the PMT face to best fit the data.

The optical parameters found by this procedure are given in the following table (units of mm where needed):

Surface	Location z	Curvature k	4th-Order A_4	6th-Order A_6
Front face of field lens	0	0.0126	-3.6	0
Rear face of field lens	7	-0.02105	0.66	0
Front face of 1st condenser	91.5	0.0126	-3.6	0
Rear face of 1st condenser	98.5	-0.02105	0.66	0
Front face of 2nd condenser	99.5	0.02105	0.66	0
Rear face of 2nd condenser	106.5	-0.0126	-3.6	0
Image plane film	146.5	0	0	0
Image plane PMT face	142	0	0	0

We do not regard these parameters as definitive, but, rather, as being representative of the departures from design values needed to fit the data.

4.2 Lens Shape

The curved surfaces of the prototype (double-convex) lenses used in this exercise were described by the manufacturer as being spherical with radii of curvature, 77 mm and 47 mm. However, these parameters do not lead to a satisfactory simulation of the test results. Therefore, measurements of the lens shape were made at DESY and the results were made available to us for this study. We fit these measurements to the description of the lens surface shape used in our ray-tracing tools,

$$h(r) = \frac{1}{k}\left[1 - \sqrt{1 - (kr)^2} + \frac{A_4}{8}(kr)^4 + \frac{A_6}{16}(kr)^6\right]$$

where h is the height of the surface from a plane normal to it at its center, r is the radial distance from the center of the surface, k is the curvature parameter ($k = 1/R$ for spherical surfaces), A_4 is the 4th-order correction

term, and A_6 is the 6th-order correction term. The coefficients of the aspherical correction terms were normalized to be the same as the corresponding terms in a Taylor-series expansion of a purely spherical surface when the corresponding A parameter is unity.

The Solver tool of MS Excel was used to fit the shape measurements with the parameters used here. Purely spherical surfaces yield residuals of nearly 100 microns, which we consider to be unsatisfactory. Good fits are obtained if we include the A_4 term; the corresponding residuals are less than 10 microns. Because of the limited number and range of surface measurements, we chose not to include an A_6 term in the fits used in this simulation study. The shape parameters determined from these fits and used in the simulation are given in the table above.

4.3   Photographic Image

To begin to understand the optics of the experimental setup, we studied the film-image that was taken with red laser light (with small angular divergence) parallel to the optic axis falling on a 2 mm-pitch grating (rectangular array of 1 mm lines spaced by 1mm.) that was placed in front of the field lens—see Figure 10, above. The "local" magnification across this image was determined by measuring the distances between spots along the $x-$ and $y-$ axes of the photograph. The local magnification is defined here as the distance between two adjacent spots divided by 2 mm, the distance between open squares on the input grating. (Our sign convention is for all axes to point in the same direction. Because this optical arrangement reverses images, the magnification is a negative number.) We choose to plot this quantity rather than the ratio of final position to initial position because it is sensitive to distortions in the image. The local magnification is plotted versus initial amplitude of the ray in Figure 16.

Data taken along the two axes are consistent and show the aberrations expected for this kind of optical system. Our simulation of the local magnification, using parameters determined in this study, is also shown in the figure. To achieve strong-enough de-magnification at zero-initial amplitude, it was necessary to increase the distance between the field lens and first condenser by 0.5 mm from the design value. The local magnification at large initial amplitudes is sensitive to the z-position of the observing film; the simulated position was varied to conform to the data shown in Figure 16. The best "eye-ball" fit gives $z = 146.5$ mm for the location of the film plane, corresponding to 40 mm behind the second condenser or about 2 mm *behind* the design location.
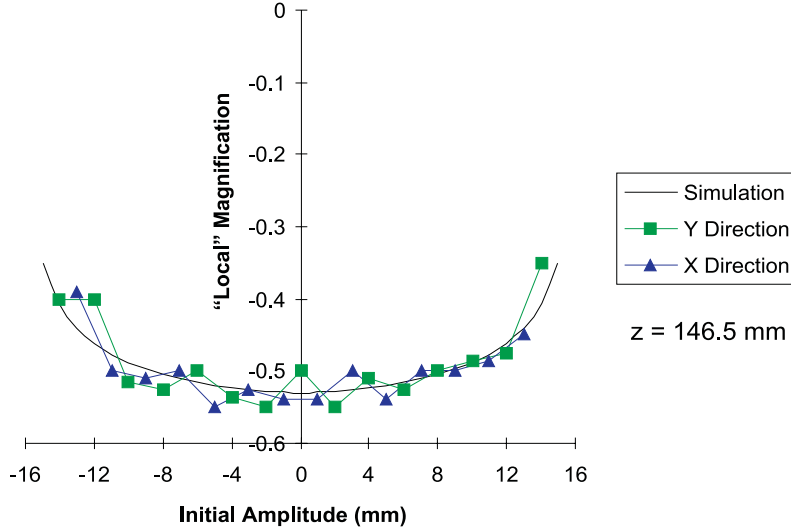
25

Figure 16: Local magnification vs Initial Amplitude determined by measurements of image photograph taken with parallel rays. z refers to the location of the film plane relative to the front surface of the field lens.

With these parameters, the pattern of spots on the photograph was simulated by single rays launched parallel to the system axis on a 2 mm grid. The photograph, itself, was digitized with an HP scanner and the resulting image was processed to keep the exposed spots. The scanning and image-processing retained the spatial relationships and scale of the photograph. The simulated rays were then overlaid on the film image and positioned to give the best overall match. The pattern of simulated rays was symmetric with respect to the origin—the photographic spots need not have the same symmetry, meaning that our simulated rays need not correspond to the exact center of the spots, which they do not.

The agreement between the photograph—see Figure 10—and simulation is quite good, even at the edge of the image, where the imaging properties are highly non-linear. With the exception of two or three rays on the very periphery, every simulated ray corresponds to an illuminated spot on the film and the locations of rays relative to their corresponding spots are nearly consistent across the entire field.

4.4 Studies of Optical Quality

As described above, the optical quality of the prototype telescope was studied by illuminating spots at 0, 7.5 mm, and 15 mm from the optic axis on the field lens with rays incident over a range of angles and recording the corresponding locations on the image plane. Simulations of Figures 7, 8, and 9 are given below.
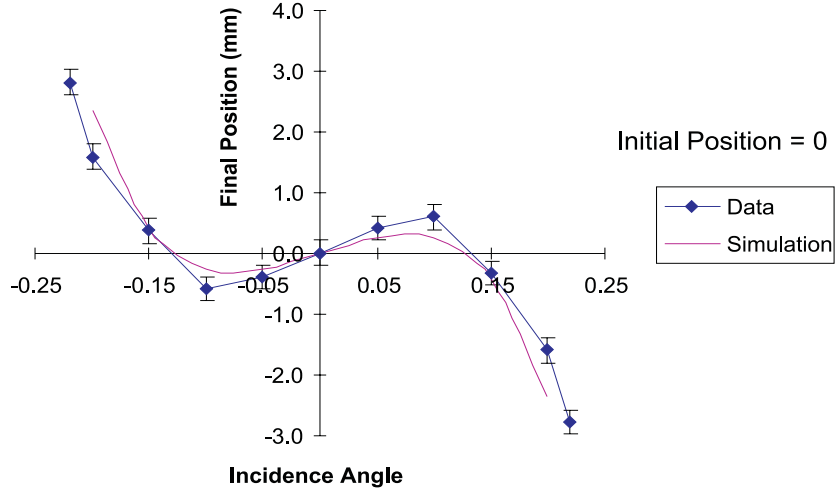

Figure 17: Data from Figure 7 above with results of simulation.

In our simulations of the optical-quality studies, single rays were tracked and the image location was varied to match the slope of the position vs angle curve at zero-incidence angle. This slope, for small amplitudes, is just the position/angle element of the linear transport matrix,

$$M_{x_f x_i'} = (z - z_{\text{focus}})/m$$

where m is the magnification of the optical system, -0.53 in this case, and $z - z_{\text{focus}}$ is the distance of the observing screen from the paraxial focus. It turns out that the same image location is indicated for these studies as was found earlier for the photographic image.

The small-amplitude data—0 mm and 7.5 mm—are reasonably well described by the simulation, but we were not always able to successfully track rays at the largest angles used in the measurements. We speculate that the non-zero beam size and divergence, and non-linear response of the eye to changes in intensity are responsible for these apparent discrepancies.
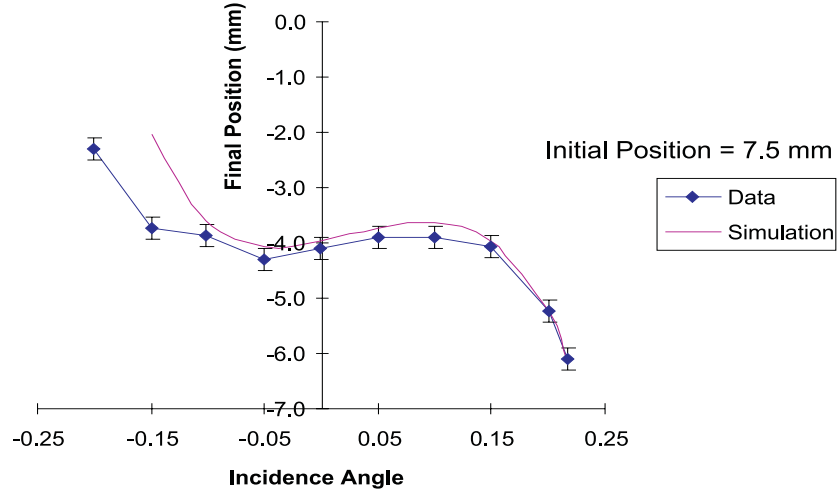
27

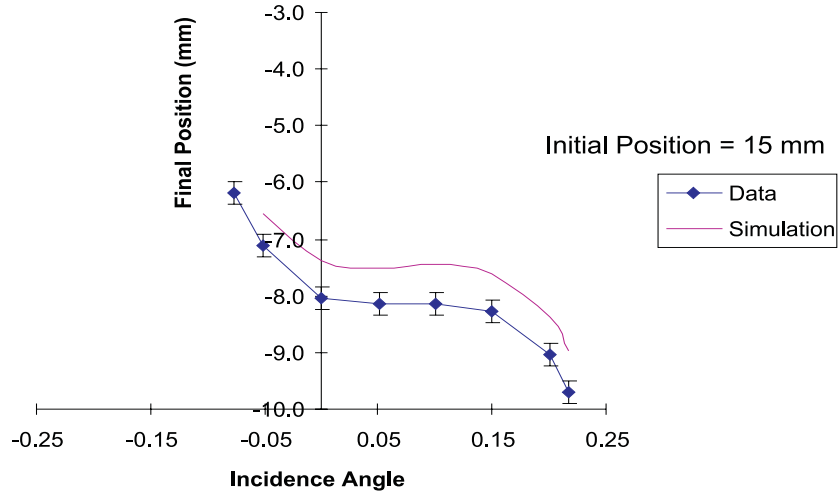Figure 18: Data from Figure 8 above with results of simulation.

Figure 19: Data from Figure 9 above with results of simulation.

The large-amplitude data of Figure 19, however, are reproduced in shape, but not in magnitude. Indeed, we can see from the data, alone, that the final position — > 8 mm — for zero-angle rays striking the field lens at 15 mm presented in Figure 9 above (Figure 19 here) is inconsistent with the photograph discussed above (where all spots are inside a radius of 8 mm), if the two measurements were taken at the same longitudinal position.

The paper states that the optical quality measurement was performed at a smaller longitudinal position, which may account for the larger data values in Figure 19, but would seem to be inconsistent with the data for smaller initial amplitudes, shown here in Figures 17 and 18, where the shape and magnitude of the curves suggest the larger $z-$position. Assuming the film plane really was at the same z-location as the image plane used in these studies, we can "count spots" on the photograph and see that the final position would be 7.5 mm, as expected from the simulation. We do not understand the discrepancy implied in Figure 19.

4.5 Cell Efficiencies

The third test done was to simulate the efficiency data shown in Figure 11. In the simulation, 10,000 rays were launched onto the first quadrant of a circle 17.95 mm in radius, matching the aperture reported for the experimental setup. We studied the response in the third quadrant of the PMT, namely, cells labeled 2, 3 and 6 in Figure 2.

With no light-collector in place, we would expect the number of rays hitting each 4.5 mm square PMT cell, N_c, to be related to the number of rays generated, N_0, by the ratio of areas:

$$N_c = N_0 \frac{1}{4} \frac{\pi r^2}{4.5^2} \approx 0.02 N_0$$

Inserting an ideal light collector with a magnification of 0.5, one would expect four times that number of rays striking each cell. Consequently, the data are presented as the ratio of the number of surviving rays with a light collector in place to four-times the number of rays striking a cell when the light collector is removed. This ratio is called the "collection-efficiency" in the discussion above and in Figure 20, below. Obviously, a simple factor of four does not account for absorption and reflections, so one would not expect the collection efficiency defined in this way to be unity, even with perfect optics.

The curves shown in Figure 20 are results of the simulation; data from the measurements discussed previously are presented as points. The statistical error on the simulated collection efficiencies is less than 0.05.

The same lens shapes and positions were used in this simulation as in the earlier sections, with the exception that the longitudinal position of the PMT face was varied to better fit the data. The curves in Figure 20 assume the PMT face is 35.5 mm from the exit of the second condenser lens. The PMT face is assumed to be 1.2 mm thick glass. The transmission of the lens
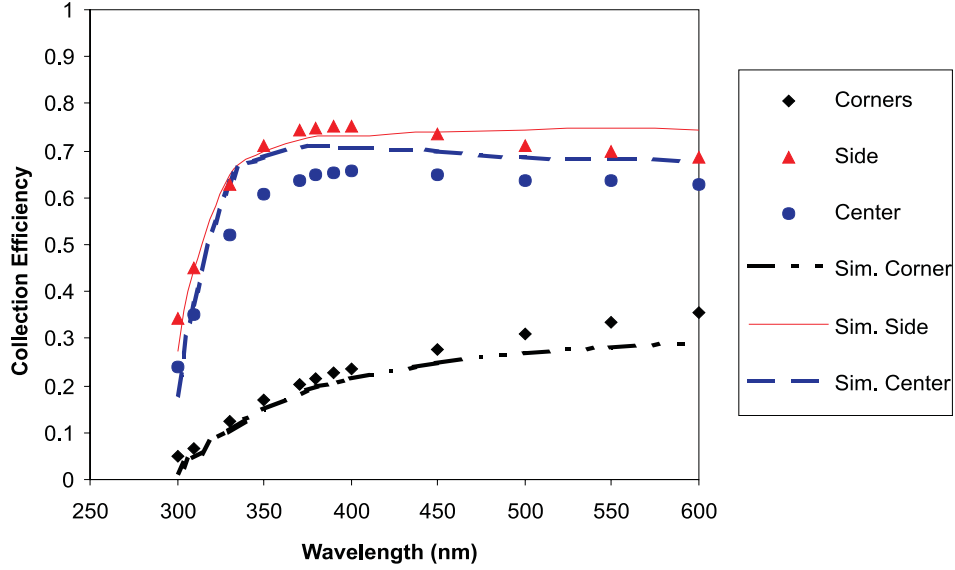
Figure 20: Data on cell transmission efficiency plotted versus wavelength taken from Figure 11 above along with the results of this simulation.

material used in the simulation is taken from the paper referenced before, *Measurements of Transmission of Plastic*.

While not perfect, the simulation reproduces the data quite well. The corner cell is least well-described by the model. Examination of the photograph of Figure 10 shows that corner PMT cells are barely covered by typical images formed in the present setup and, therefore, are the ones most sensitive to variations in the details of the optics or uniformity of response of the PMT.

In summary, most of the important features of the measurements performed on the prototype light collectors can be described adequately by a set of parameters that are reasonably close to values expected from independent determinations. This is significant because the optics used in the prototype measurements are pushed far beyond the linear regime. We conclude from this work that our simulation tools are capable of detailed modeling of lens-based light collectors planned for the Hera-B RICH, where the optical behavior is considerably more linear than that of the prototype telescope described in this note.